

Branching fraction measurements of $\psi(3686) \rightarrow \gamma\chi_{cJ}$

M. Ablikim¹, M. N. Achasov^{9,e}, S. Ahmed¹⁴, M. Albrecht⁴, A. Amoroso^{50A,50C}, F. F. An¹, Q. An^{47,a}, J. Z. Bai¹, O. Bakina²⁴, R. Baldini Ferroli^{20A}, Y. Ban³², D. W. Bennett¹⁹, J. V. Bennett⁵, N. Berger²³, M. Bertani^{20A}, D. Bettoni^{21A}, J. M. Bian⁴⁵, F. Bianchi^{50A,50C}, E. Boger^{24,c}, I. Boyko²⁴, R. A. Briere⁵, H. Cai⁵², X. Cai^{1,a}, O. Cakir^{42A}, A. Calcaterra^{20A}, G. F. Cao¹, S. A. Cetin^{42B}, J. Chai^{50C}, J. F. Chang^{1,a}, G. Chelkov^{24,c,d}, G. Chen¹, H. S. Chen¹, J. C. Chen¹, M. L. Chen^{1,a}, S. J. Chen³⁰, X. R. Chen²⁷, Y. B. Chen^{1,a}, X. K. Chu³², G. Cibinetto^{21A}, H. L. Dai^{1,a}, J. P. Dai^{35,j}, A. Dbeysli¹⁴, D. Dedovich²⁴, Z. Y. Deng¹, A. Denig²³, I. Denysenko²⁴, M. Destefanis^{50A,50C}, F. De Mori^{50A,50C}, Y. Ding²⁸, C. Dong³¹, J. Dong^{1,a}, L. Y. Dong¹, M. Y. Dong^{1,a}, O. Dorjkhaidav²², Z. L. Dou³⁰, S. X. Du⁵⁴, P. F. Duan¹, J. Fang^{1,a}, S. S. Fang¹, X. Fang^{47,a}, Y. Fang¹, R. Farinelli^{21A,21B}, L. Fava^{50B,50C}, S. Fegan²³, F. Feldbauer²³, G. Felici^{20A}, C. Q. Feng^{47,a}, E. Fioravanti^{21A}, M. Fritsch^{14,23}, C. D. Fu¹, Q. Gao¹, X. L. Gao^{47,a}, Y. Gao⁴¹, Y. G. Gao⁶, Z. Gao^{47,a}, I. Garzia^{21A}, K. Goetzen¹⁰, L. Gong³¹, W. X. Gong^{1,a}, W. Gradl²³, M. Greco^{50A,50C}, M. H. Gu^{1,a}, S. Gu¹⁵, Y. T. Gu¹², A. Q. Guo¹, L. B. Guo²⁹, R. P. Guo¹, Y. P. Guo²³, Z. Haddadi²⁶, S. Han⁵², X. Q. Hao¹⁵, F. A. Harris⁴⁴, K. L. He¹, X. Q. He⁴⁶, F. H. Heinsius⁴, T. Held⁴, Y. K. Heng^{1,a}, T. Holtmann⁴, Z. L. Hou¹, C. Hu²⁹, H. M. Hu¹, T. Hu^{1,a}, Y. Hu¹, G. S. Huang^{47,a}, J. S. Huang¹⁵, X. T. Huang³⁴, X. Z. Huang³⁰, Z. L. Huang²⁸, T. Hussain⁴⁹, W. Ikegami Andersson⁵¹, Q. Ji¹, Q. P. Ji¹⁵, X. B. Ji¹, X. L. Ji^{1,a}, X. S. Jiang^{1,a}, X. Y. Jiang³¹, J. B. Jiao³⁴, Z. Jiao¹⁷, D. P. Jin^{1,a}, S. Jin¹, T. Johansson⁵¹, A. Julin⁴⁵, N. Kalantar-Nayestanaki²⁶, X. L. Kang¹, X. S. Kang³¹, M. Kavatsyuk²⁶, B. C. Ke⁵, T. Khan^{47,a}, P. Kiese²³, R. Kliemt¹⁰, L. Koch²⁵, O. B. Kolcu^{42B,h}, B. Kopf⁴, M. Kornicer⁴⁴, M. Kuemmel⁴, M. Kuhlmann⁴, A. Kupsc⁵¹, W. Kühn²⁵, J. S. Lange²⁵, M. Lara¹⁹, P. Larin¹⁴, L. Lavezzi^{50C,1}, H. Leithoff²³, C. Leng^{50C}, C. Li⁵¹, Cheng Li^{47,a}, D. M. Li⁵⁴, F. Li^{1,a}, F. Y. Li³², G. Li¹, H. B. Li¹, H. J. Li¹, J. C. Li¹, Jin Li³³, K. Li¹³, K. Li³⁴, Lei Li³, P. L. Li^{47,a}, P. R. Li^{7,43}, Q. Y. Li³⁴, T. Li³⁴, W. D. Li¹, W. G. Li¹, X. L. Li³⁴, X. N. Li^{1,a}, X. Q. Li³¹, Z. B. Li⁴⁰, H. Liang^{47,a}, Y. F. Liang³⁷, Y. T. Liang²⁵, G. R. Liao¹¹, D. X. Lin¹⁴, B. Liu^{35,j}, B. J. Liu¹, C. X. Liu¹, D. Liu^{47,a}, F. H. Liu³⁶, Fang Liu¹, Feng Liu⁶, H. B. Liu¹², H. H. Liu¹⁶, H. H. Liu¹, H. M. Liu¹, J. B. Liu^{47,a}, J. P. Liu⁵², J. Y. Liu¹, K. Liu⁴¹, K. Y. Liu²⁸, Ke Liu⁶, L. D. Liu³², P. L. Liu^{1,a}, Q. Liu⁴³, S. B. Liu^{47,a}, X. Liu²⁷, Y. B. Liu³¹, Y. Y. Liu³¹, Z. A. Liu^{1,a}, Zhiqing Liu²³, Y. F. Long³², X. C. Lou^{1,a,g}, H. J. Lu¹⁷, J. G. Lu^{1,a}, Y. Lu¹, Y. P. Lu^{1,a}, C. L. Luo²⁹, M. X. Luo⁵³, T. Luo⁴⁴, X. L. Luo^{1,a}, X. R. Lyu⁴³, F. C. Ma²⁸, H. L. Ma¹, L. L. Ma³⁴, M. M. Ma¹, Q. M. Ma¹, T. Ma¹, X. N. Ma³¹, X. Y. Ma^{1,a}, Y. M. Ma³⁴, F. E. Maas¹⁴, M. Maggiora^{50A,50C}, Q. A. Malik⁴⁹, Y. J. Mao³², Z. P. Mao¹, S. Marcello^{50A,50C}, J. G. Messchendorp²⁶, G. Mezzadri^{21B}, J. Min^{1,a}, T. J. Min¹, R. E. Mitchell¹⁹, X. H. Mo^{1,a}, Y. J. Mo⁶, C. Morales Morales¹⁴, G. Morello^{20A}, N. Yu. Muchnoi^{9,e}, H. Muramatsu⁴⁵, P. Musiol⁴, A. Mustafa⁴, Y. Nefedov²⁴, F. Nerling¹⁰, I. B. Nikolaev^{9,e}, Z. Ning^{1,a}, S. Nisar⁸, S. L. Niu^{1,a}, X. Y. Niu¹, S. L. Olsen³³, Q. Ouyang^{1,a}, S. Pacetti^{20B}, Y. Pan^{47,a}, P. Patteri^{20A}, M. Pelizaeus⁴, J. Pellegrino^{50A,50C}, H. P. Peng^{47,a}, K. Peters^{10,i}, J. Pettersson⁵¹, J. L. Ping²⁹, R. G. Ping¹, R. Poling⁴⁵, V. Prasad^{39,47}, H. R. Qi², M. Qi³⁰, S. Qian^{1,a}, C. F. Qiao⁴³, J. J. Qin⁴³, N. Qin⁵², X. S. Qin¹, Z. H. Qin^{1,a}, J. F. Qiu¹, K. H. Rashid⁴⁹, C. F. Redmer²³, M. Richter⁴, M. Ripka²³, G. Rong¹, Ch. Rosner¹⁴, X. D. Ruan¹², A. Sarantsev^{24,f}, M. Savrie^{21B}, C. Schnier⁴, K. Schoenning⁵¹, W. Shan³², M. Shao^{47,a}, C. P. Shen², P. X. Shen³¹, X. Y. Shen¹, H. Y. Sheng¹, J. J. Song³⁴, X. Y. Song¹, S. Sosio^{50A,50C}, C. Sowa⁴, S. Spataro^{50A,50C}, G. X. Sun¹, J. F. Sun¹⁵, S. S. Sun¹, X. H. Sun¹, Y. J. Sun^{47,a}, Y. K. Sun^{47,a}, Y. Z. Sun¹, Z. J. Sun^{1,a}, Z. T. Sun¹⁹, C. J. Tang³⁷, G. Y. Tang¹, X. Tang¹, I. Tapan^{42C}, M. Tiemens²⁶, B. T. Tsednee²², I. Uman^{42D}, G. S. Varner⁴⁴, B. Wang¹, B. L. Wang⁴³, D. Wang³², D. Y. Wang³², Dan Wang⁴³, K. Wang^{1,a}, L. L. Wang¹, L. S. Wang¹, M. Wang³⁴, P. Wang¹, P. L. Wang¹, W. P. Wang^{47,a}, X. F. Wang⁴¹, Y. D. Wang¹⁴, Y. F. Wang^{1,a}, Y. Q. Wang²³, Z. Wang^{1,a}, Z. G. Wang^{1,a}, Z. H. Wang^{47,a}, Z. Y. Wang¹, Z. Y. Wang¹, T. Weber²³, D. H. Wei¹¹, P. Weidenkaff²³, S. P. Wen¹, U. Wiedner⁴, M. Wolke⁵¹, L. H. Wu¹, L. J. Wu¹, Z. Wu^{1,a}, L. Xia^{47,a}, Y. Xia¹⁸, D. Xiao¹, H. Xiao⁴⁸, Y. J. Xiao¹, Z. J. Xiao²⁹, Y. G. Xie^{1,a}, Y. H. Xie⁶, X. A. Xiong¹, Q. L. Xiu^{1,a}, G. F. Xu¹, J. J. Xu¹, L. Xu¹, Q. J. Xu¹³, Q. N. Xu⁴³, X. P. Xu³⁸, L. Yan^{50A,50C}, W. B. Yan^{47,a}, W. C. Yan^{47,a}, Y. H. Yan¹⁸, H. J. Yang^{35,j}, H. X. Yang¹, L. Yang⁵², Y. H. Yang³⁰, Y. X. Yang¹¹, M. Ye^{1,a}, M. H. Ye⁷, J. H. Yin¹, Z. Y. You⁴⁰, B. X. Yu^{1,a}, C. X. Yu³¹, J. S. Yu²⁷, C. Z. Yuan¹, Y. Yuan¹, A. Yuncu^{42B,b}, A. A. Zafar⁴⁹, Y. Zeng¹⁸, Z. Zeng^{47,a}, B. X. Zhang¹, B. Y. Zhang^{1,a}, C. C. Zhang¹, D. H. Zhang¹, H. H. Zhang⁴⁰, H. Y. Zhang^{1,a}, J. Zhang¹, J. L. Zhang¹, J. Q. Zhang¹, J. W. Zhang^{1,a}, J. Y. Zhang¹, J. Z. Zhang¹, K. Zhang¹, L. Zhang⁴¹, S. Q. Zhang³¹, X. Y. Zhang³⁴, Y. Zhang¹, Y. Zhang¹, Y. H. Zhang^{1,a}, Y. T. Zhang^{47,a}, Yu Zhang⁴³, Z. H. Zhang⁶, Z. P. Zhang⁴⁷, Z. Y. Zhang⁵², G. Zhao¹, J. W. Zhao^{1,a}, J. Y. Zhao¹, J. Z. Zhao^{1,a}, Lei Zhao^{47,a}, Ling Zhao¹, M. G. Zhao³¹, Q. Zhao¹, S. J. Zhao⁵⁴, T. C. Zhao¹, Y. B. Zhao^{1,a}, Z. G. Zhao^{47,a}, A. Zhemchugov^{24,c}, B. Zheng^{14,48}, J. P. Zheng^{1,a}, W. J. Zheng³⁴, Y. H. Zheng⁴³, B. Zhong²⁹, L. Zhou^{1,a}, X. Zhou⁵², X. K. Zhou^{47,a}, X. R. Zhou^{47,a}, X. Y. Zhou¹, Y. X. Zhou^{12,a}, K. Zhu¹, K. J. Zhu^{1,a}, S. Zhu¹, S. H. Zhu⁴⁶, X. L. Zhu⁴¹, Y. C. Zhu^{47,a}, Y. S. Zhu¹, Z. A. Zhu¹, J. Zhuang^{1,a}, L. Zotti^{50A,50C}, B. S. Zou¹, J. H. Zou¹

(BESIII Collaboration)

¹ Institute of High Energy Physics, Beijing 100049, People's Republic of China

² Beihang University, Beijing 100191, People's Republic of China

³ Beijing Institute of Petrochemical Technology, Beijing 102617, People's Republic of China

⁴ Bochum Ruhr-University, D-44780 Bochum, Germany

⁵ Carnegie Mellon University, Pittsburgh, Pennsylvania 15213, USA

⁶ Central China Normal University, Wuhan 430079, People's Republic of China

⁷ China Center of Advanced Science and Technology, Beijing 100190, People's Republic of China

⁸ COMSATS Institute of Information Technology, Lahore, Defence Road, Off Raiwind Road, 54000 Lahore, Pakistan

⁹ G.I. Budker Institute of Nuclear Physics SB RAS (BINP), Novosibirsk 630090, Russia

¹⁰ GSI Helmholtzcentre for Heavy Ion Research GmbH, D-64291 Darmstadt, Germany

- ¹¹ Guangxi Normal University, Guilin 541004, People's Republic of China
- ¹² Guangxi University, Nanning 530004, People's Republic of China
- ¹³ Hangzhou Normal University, Hangzhou 310036, People's Republic of China
- ¹⁴ Helmholtz Institute Mainz, Johann-Joachim-Becher-Weg 45, D-55099 Mainz, Germany
- ¹⁵ Henan Normal University, Xinxiang 453007, People's Republic of China
- ¹⁶ Henan University of Science and Technology, Luoyang 471003, People's Republic of China
- ¹⁷ Huangshan College, Huangshan 245000, People's Republic of China
- ¹⁸ Hunan University, Changsha 410082, People's Republic of China
- ¹⁹ Indiana University, Bloomington, Indiana 47405, USA
- ²⁰ (A)INFN Laboratori Nazionali di Frascati, I-00044, Frascati, Italy; (B)INFN and University of Perugia, I-06100, Perugia, Italy
- ²¹ (A)INFN Sezione di Ferrara, I-44122, Ferrara, Italy; (B)University of Ferrara, I-44122, Ferrara, Italy
- ²² Institute of Physics and Technology, Peace Ave. 54B, Ulaanbaatar 13330, Mongolia
- ²³ Johannes Gutenberg University of Mainz, Johann-Joachim-Becher-Weg 45, D-55099 Mainz, Germany
- ²⁴ Joint Institute for Nuclear Research, 141980 Dubna, Moscow region, Russia
- ²⁵ Justus-Liebig-Universitaet Giessen, II. Physikalisches Institut, Heinrich-Buff-Ring 16, D-35392 Giessen, Germany
- ²⁶ KVI-CART, University of Groningen, NL-9747 AA Groningen, The Netherlands
- ²⁷ Lanzhou University, Lanzhou 730000, People's Republic of China
- ²⁸ Liaoning University, Shenyang 110036, People's Republic of China
- ²⁹ Nanjing Normal University, Nanjing 210023, People's Republic of China
- ³⁰ Nanjing University, Nanjing 210093, People's Republic of China
- ³¹ Nankai University, Tianjin 300071, People's Republic of China
- ³² Peking University, Beijing 100871, People's Republic of China
- ³³ Seoul National University, Seoul, 151-747 Korea
- ³⁴ Shandong University, Jinan 250100, People's Republic of China
- ³⁵ Shanghai Jiao Tong University, Shanghai 200240, People's Republic of China
- ³⁶ Shanxi University, Taiyuan 030006, People's Republic of China
- ³⁷ Sichuan University, Chengdu 610064, People's Republic of China
- ³⁸ Soochow University, Suzhou 215006, People's Republic of China
- ³⁹ State Key Laboratory of Particle Detection and Electronics, Beijing 100049, Hefei 230026, People's Republic of China
- ⁴⁰ Sun Yat-Sen University, Guangzhou 510275, People's Republic of China
- ⁴¹ Tsinghua University, Beijing 100084, People's Republic of China
- ⁴² (A)Ankara University, 06100 Tandogan, Ankara, Turkey; (B)Istanbul Bilgi University, 34060 Eyup, Istanbul, Turkey; (C)Uludag University, 16059 Bursa, Turkey; (D)Near East University, Nicosia, North Cyprus, Mersin 10, Turkey
- ⁴³ University of Chinese Academy of Sciences, Beijing 100049, People's Republic of China
- ⁴⁴ University of Hawaii, Honolulu, Hawaii 96822, USA
- ⁴⁵ University of Minnesota, Minneapolis, Minnesota 55455, USA
- ⁴⁶ University of Science and Technology Liaoning, Anshan 114051, People's Republic of China
- ⁴⁷ University of Science and Technology of China, Hefei 230026, People's Republic of China
- ⁴⁸ University of South China, Hengyang 421001, People's Republic of China
- ⁴⁹ University of the Punjab, Lahore-54590, Pakistan
- ⁵⁰ (A)University of Turin, I-10125, Turin, Italy; (B)University of Eastern Piedmont, I-15121, Alessandria, Italy; (C)INFN, I-10125, Turin, Italy
- ⁵¹ Uppsala University, Box 516, SE-75120 Uppsala, Sweden
- ⁵² Wuhan University, Wuhan 430072, People's Republic of China
- ⁵³ Zhejiang University, Hangzhou 310027, People's Republic of China
- ⁵⁴ Zhengzhou University, Zhengzhou 450001, People's Republic of China
- ^a Also at State Key Laboratory of Particle Detection and Electronics, Beijing 100049, Hefei 230026, People's Republic of China
- ^b Also at Bogazici University, 34342 Istanbul, Turkey
- ^c Also at the Moscow Institute of Physics and Technology, Moscow 141700, Russia
- ^d Also at the Functional Electronics Laboratory, Tomsk State University, Tomsk, 634050, Russia
- ^e Also at the Novosibirsk State University, Novosibirsk, 630090, Russia
- ^f Also at the NRC "Kurchatov Institute, PNPI, 188300, Gatchina, Russia
- ^g Also at University of Texas at Dallas, Richardson, Texas 75083, USA
- ^h Also at Istanbul Arel University, 34295 Istanbul, Turkey
- ⁱ Also at Goethe University Frankfurt, 60323 Frankfurt am Main, Germany
- ^j Also at Key Laboratory for Particle Physics, Astrophysics and Cosmology, Ministry of Education; Shanghai Key Laboratory for Particle Physics and Cosmology; Institute of Nuclear and Particle Physics, Shanghai 200240, People's Republic of China

(Dated: June 15, 2021)

Using a sample of 106 million $\psi(3686)$ decays, the branching fractions of $\psi(3686) \rightarrow \gamma\chi_{c0}, \psi(3686) \rightarrow \gamma\chi_{c1}$, and $\psi(3686) \rightarrow \gamma\chi_{c2}$ are measured with improved precision to be $(9.389 \pm 0.014 \pm 0.332) \%$, $(9.905 \pm 0.011 \pm 0.353) \%$, and $(9.621 \pm 0.013 \pm 0.272) \%$, respectively, where the first uncertainties are statistical and the second ones are systematic. The product branching

fractions of $\psi(3686) \rightarrow \gamma\chi_{c1}, \chi_{c1} \rightarrow \gamma J/\psi$ and $\psi(3686) \rightarrow \gamma\chi_{c2}, \chi_{c2} \rightarrow \gamma J/\psi$ and the branching fractions of $\chi_{c1} \rightarrow \gamma J/\psi$ and $\chi_{c2} \rightarrow \gamma J/\psi$ are also presented.

PACS numbers: 13.20Gd, 13.40Hq, 14.40Pq

I. INTRODUCTION

The discovery of the J/ψ in 1974 and soon thereafter of the charmonium family convinced physicists of the reality of the quark model [1]. Since then, measurements of the masses and widths of the charmonium family and their hadronic and radiative transition branching fractions have become more precise. The spectrum of bound charmonium states is important for the understanding of Quantum Chromodynamics (QCD) in the perturbative and non-perturbative regions [2].

For charmonium states that are above the ground state but below threshold for strong decay into heavy flavored mesons, like the $\psi(3686)$, electromagnetic decays are important decay modes. The first charmonium states discovered after the J/ψ and $\psi(3686)$ were the χ_{cJ} ($J = 0, 1, \text{ and } 2$) states, which were found in radiative transitions of the $\psi(3686)$ [3, 4]. These states, which are the triplet $1P$ states of the $c\bar{c}$ system, had been theoretically predicted [5, 6] along with the suggestion that they could be produced by $E1$ transitions from the $\psi(3686)$ resonance.

Radiative transitions are sensitive to the inner structure of hadrons, and experimental progress and theoretical progress are important for understanding this structure. The development of theoretical models is also important for predicting the properties of missing charmonium states, in order to help untangle charmonium states above the open-charm threshold from the mysterious XYZ states [7]. Much information on radiative transitions of charmonium can be found in Ref. [2], and a recent summary of theoretical predictions for radiative transitions of charmonium states and comparisons with experiment may be found in Ref. [8].

The branching fractions of $\psi(3686) \rightarrow \gamma\chi_{cJ}$ were measured most recently by CLEO in 2004 with a sample of 1.6 M $\psi(3686)$ decays [9]. The Crystal Ball [10], CLEO values, and the Particle Data Group (PDG) [7] averages are given in Table I.

TABLE I. Crystal Ball [10] and CLEO [9] $\psi(3686) \rightarrow \gamma\chi_{cJ}$ branching fractions and average values from the PDG [7].

Decay	Crystal Ball (%)	CLEO (%)	PDG (%)
$\psi(3686) \rightarrow \gamma\chi_{c0}$	$9.9 \pm 0.5 \pm 0.8$	$9.22 \pm 0.11 \pm 0.46$	9.2 ± 0.4
$\psi(3686) \rightarrow \gamma\chi_{c1}$	$9.0 \pm 0.5 \pm 0.7$	$9.07 \pm 0.11 \pm 0.54$	8.9 ± 0.5
$\psi(3686) \rightarrow \gamma\chi_{c2}$	$8.0 \pm 0.5 \pm 0.7$	$9.33 \pm 0.14 \pm 0.61$	8.8 ± 0.5

BESIII has the world's largest sample of $\psi(3686)$ decays and has made precision measurements of many $\psi(3686)$ branching fractions, including $\psi(3686) \rightarrow \pi^+\pi^-J/\psi$, along with $J/\psi \rightarrow l^+l^-$ ($l = e, \mu$) [11], $\psi(3686) \rightarrow \pi^0 J/\psi$ and $\eta J/\psi$ [12], $\psi(3686) \rightarrow \pi^0 h_c$ [13,

14], and the product branching fractions $\mathcal{B}(\psi(3686) \rightarrow \gamma\chi_{cJ}) \times \mathcal{B}(\chi_{cJ} \rightarrow \gamma J/\psi)$ [15, 16] using exclusive $\chi_{cJ} \rightarrow \gamma J/\psi$ decays. It is important that the $\psi(3686) \rightarrow \gamma\chi_{cJ}$ and $\psi(3686) \rightarrow \gamma\eta_c$ branching fractions be measured as well. Improved precision on these is necessary because they are often used in the determination of χ_{cJ} and η_c branching fractions via the product branching fractions. However, it is to be noted that systematic uncertainties dominate the measurements summarized in Table I, so to improve on their results, it is necessary to reduce the systematic uncertainties.

In this paper, we analyze $\psi(3686)$ inclusive radiative decays and report the measurement of the $\psi(3686) \rightarrow \gamma\chi_{cJ}$ branching fractions. The product branching fractions $\mathcal{B}(\psi(3686) \rightarrow \gamma\chi_{cJ}) \times \mathcal{B}(\chi_{cJ} \rightarrow \gamma J/\psi)$ are also measured, and the $\chi_{cJ} \rightarrow \gamma J/\psi$ branching fractions are determined. This analysis is based on the $\psi(3686)$ event sample taken in 2009 of 106 million events, determined from the number of hadronic decays as described in Ref. [17], the corresponding continuum sample with integrated luminosity of 44 pb^{-1} at $\sqrt{s} = 3.65 \text{ GeV}$ [17], and a 106 million $\psi(3686)$ inclusive Monte Carlo (MC) sample.

The paper is organized as follows: In Section II, the BESIII detector and inclusive $\psi(3686)$ MC simulation are described. In Section III, the selections of inclusive $\psi(3686) \rightarrow \gamma X$ events and π^0 's are described and comparisons of inclusive $\psi(3686)$ data and MC sample distributions are made. Section IV presents the inclusive photon energy distributions, while Section V details the selection of exclusive $\psi(3686) \rightarrow \gamma\chi_{cJ}$ events. Sections VI and VII describe the fitting of the photon energy distributions and the determination of the branching fractions, respectively. Section VIII presents the systematic uncertainties, and Sections IX and X give the results and summary, respectively.

II. BESIII AND INCLUSIVE $\psi(3686)$ MONTE CARLO SIMULATION

BESIII is a general-purpose detector at the double-ring e^+e^- collider BEPCII and is used for the study of physics in the τ -charm energy region [18]. It has a geometrical acceptance of 93% of 4π solid angle and consists of four main subsystems: a helium-based multi-layer drift chamber (MDC), a plastic scintillator time-of-flight (TOF) system, a CsI(Tl) electromagnetic calorimeter (EMC) and a resistive plate muon chamber system. The first three sub-detectors are enclosed in a superconducting solenoidal magnet with a 1.0 T magnetic field. More details of the detector are described in Ref. [19].

MC simulations of the full detector are used to de-

termine detection efficiency and to understand potential backgrounds. The GEANT4-based [20] simulation software, BESIII Object Oriented Simulation [21], contains the detector geometry and material description, the detector response and signal digitization models, as well as records of the detector running conditions and performance. Effects of initial state radiation (ISR) are taken into account with the MC event generator KKMC [22, 23], and final state radiation (FSR) effects are included in the simulation by using PHOTOS [24]. Particle decays are simulated with EVTGEN [25] for the known decay modes with branching fractions set to the world average [7] and with the LUNDCHARM model [26] for the remaining unknown decays.

Angular distributions of the cascade $E1$ transitions $\psi(3686) \rightarrow \gamma\chi_{cJ}$ follow the formulas in Refs. [27, 28], while the $\cos\theta$ distributions for $\chi_{cJ} \rightarrow \gamma J/\psi$ are generated according to phase space distributions. The χ_{cJ} are simulated with Breit-Wigner line shapes. To account for the $E1$ transitions for $\psi(3686) \rightarrow \gamma\chi_{cJ}, \chi_{cJ} \rightarrow \gamma J/\psi$, MC events will be weighted as described in Section IV.

III. EVENT SELECTION

A. Inclusive $\psi(3686) \rightarrow \gamma X$ Event Selection

We start by describing the selection procedure for $\psi(3686)$ event candidates. To minimize systematic uncertainties from selection requirements, the $\psi(3686)$ event selection criteria, which are used for both data and the MC sample, are fairly loose.

Charged tracks must be in the active region of the MDC with $|\cos\theta| < 0.93$, where θ is the polar angle of the track, and have $V_r < 2$ cm and $|V_z| < 10$ cm, where V_r is the distance of the point of closest approach of the track to the beam line in the plane perpendicular to the beam line and $|V_z|$ is the distance to the point of closest approach from the interaction point along the beam direction. In addition, $p < 2.0$ GeV/ c is required to eliminate misreconstructed tracks, where p is the track momentum.

Photon candidates are reconstructed from clusters of energy in the EMC that are separated from the extrapolated positions of any charged tracks by more than 10 standard deviations and have reconstructed energy $E_\gamma > 25$ MeV in the EMC barrel ($|\cos\theta_\gamma| < 0.80$) or > 50 MeV in the EMC end-caps ($0.86 < |\cos\theta_\gamma| < 0.92$), where E_γ is the photon energy and θ_γ is the polar angle of the photon. The energy deposited in nearby TOF counters is included in EMC measurements to improve the reconstruction efficiency and energy resolution. Photons in the region between the barrel and end-caps are poorly reconstructed and are not used. In addition, $E_\gamma < 2.0$ GeV is required to eliminate misreconstructed photons. The timing of the shower is required to be no later than 700 ns after the reconstructed event start time to suppress electronic noise and energy deposits unrelated to

the event.

To help in the selection of good $\psi(3686)$ candidates, events must have $N_{\text{ch}} > 0$, where N_{ch} is the number of charged tracks, and $E_{\text{vis}} = E_{\text{ch}} + E_{\text{neu}} > 0.22E_{\text{cm}}$, where E_{vis} is the visible energy of the event, E_{ch} is the total energy of the charged particles assuming them to be pions, E_{neu} is the total energy of the photons in the event, and E_{cm} is the center of mass (CM) energy. To remove beam background related showers in the EMC and to demand at least one photon candidate in order to select inclusive $\psi(3686) \rightarrow \gamma X$ events, we require $0 < N_\gamma < 17$, where N_γ is the number of photons. In the following, inclusive $\psi(3686)$ events and inclusive $\psi(3686)$ MC events will assume this selection.

B. Non- $\psi(3686)$ background

By examining the continuum sample taken at a CM energy of 3.65 GeV, a set of selection requirements were chosen to further remove non- $\psi(3686)$ background by identifying Bhabha events, two-photon events, ISR events, beam background events, electronic noise, etc. Events satisfying any of the following conditions will be removed:

1. $N_{\text{ch}} < 4$ and $p_i c > 0.92E_{\text{beam}}$, where E_{beam} is the beam energy and the p_i is the momentum of any charged track in the event.
2. $N_{\text{ch}} < 4$ and $(E_{\text{EMC}})_i > 0.9E_{\text{beam}}$, where $(E_{\text{EMC}})_i$ is the deposited energy of any charged or neutral track in the EMC.
3. $N_{\text{ch}} < 4$ and $E_{\text{cal}} < 0.15E_{\text{cm}}$, where E_{cal} is the total deposited energy (charged and neutral) in the EMC.
4. $N_{\text{ch}} = 1$ and $(E_{\text{ch}} + E_{\text{neu}}) < 0.35E_{\text{cm}}$.
5. $|((P_z)_{\text{ch}} + (P_z)_{\text{neu}})|c > 0.743E_{\text{beam}}$, where $(P_z)_{\text{ch}}$ and $(P_z)_{\text{neu}}$ are the sums of the momenta of the charged and neutral tracks in the z direction.

CLEO in Ref. [9] used a similar selection in their analysis.

C. π^0 candidate selection

The invariant mass distribution of all $\gamma\gamma$ combinations has a clear peak from $\pi^0 \rightarrow \gamma\gamma$ decay. To reduce background under the radiative transition peaks, photons in π^0 's will be removed from the inclusive photon energy distributions. To reduce the loss of good radiative transition photons due to accidental mis-combinations under the π^0 peak, the requirements for a π^0 candidate are rather strict.

Photons in π^0 candidates must have $\delta > 14$ degrees, where δ is the angle between the photon and the closest charged track in the event, and the lateral shower profile must be consistent with that of a single photon.

The π^0 candidates must have at least one photon in the EMC barrel; a one-constraint kinematic fit to the nominal π^0 mass with a $\chi^2 < 200$; and $0.12 < M_{\gamma\gamma} < 0.145$ GeV/ c^2 , where $M_{\gamma\gamma}$ is the $\gamma\gamma$ invariant mass. In addition, $|\cos\theta^*| < 0.84$ is required for a π^0 candidate, where θ^* is the angle of a photon in the π^0 rest frame with respect to the π^0 line of flight. Real π^0 mesons decay isotropically, and their decay angular distribution is flat. However π^0 candidates that originate from a wrong photon combination do not have a flat distribution and peak near $|\cos\theta^*| = 1$.

D. Comparison of inclusive $\psi(3686)$ data and the MC sample

Since efficiencies and backgrounds depend on the accuracy of the MC simulation, it is important to validate the simulation by comparing the inclusive $\psi(3686)$ MC with on-peak data minus continuum data. In the following, data will refer to on-peak data minus scaled continuum data, where the scale factor of 3.677 accounts for the difference in energy and luminosity between the two data sets [17]. In general, data distributions compare well with the inclusive MC distributions, except for those involving π^0 s. To improve the agreement, each MC event is given a weight determined by the number of π^0 s, N_{π^0} , in the event. For events with N_{π^0} corresponding to bin i of the N_{π^0} distribution, $w_{\pi^0} = \frac{(N_{\pi^0}^{\text{data}})_i}{(N_{\pi^0}^{\text{MC}})_i}$.

In Fig. 1 representative charged track distributions, (a) N_{ch} , (b) V_z , (c) p , and (d) E_{EMC} , are shown. Here and for the distributions of Figs. 2 and 3, data, unweighted MC, and weighted MC distributions are shown. Photon distributions, (a) N_γ , (b) θ_γ , (c) δ , and (d) $M_{\gamma\gamma}$ of all $\gamma\gamma$ combinations, are shown in Fig. 2. The agreement is acceptable for the charged distributions with or without weighting. For photons, the agreement for the π^0 peak in the $M_{\gamma\gamma}$ distribution (Fig. 2 (d)) is improved with the weighted MC distribution, while the agreement for the other distributions is neither better or worse.

Representative π^0 candidate (see Section III C) distributions, (a) the number of π^0 s (N_{π^0}), (b) the $\gamma\gamma$ invariant mass ($M_{\gamma\gamma}$) made without the π^0 mass selection requirement, (c) $|\cos\theta^*|$, and (d) momentum (P_{π^0}), are shown in Fig. 3. The agreement is improved for the weighted MC sample, and in the following, the inclusive MC distributions will be weighted by w_{π^0} .

IV. INCLUSIVE PHOTON ENERGY DISTRIBUTIONS

Inclusive photon energy distributions are obtained using the following selection requirements. First, the event must satisfy the inclusive $\psi(3686)$ selection requirements, as described in Section III A, and not be a non- $\psi(3686)$ background event, as defined in Section III B, a $\pi^+\pi^-J/\psi$

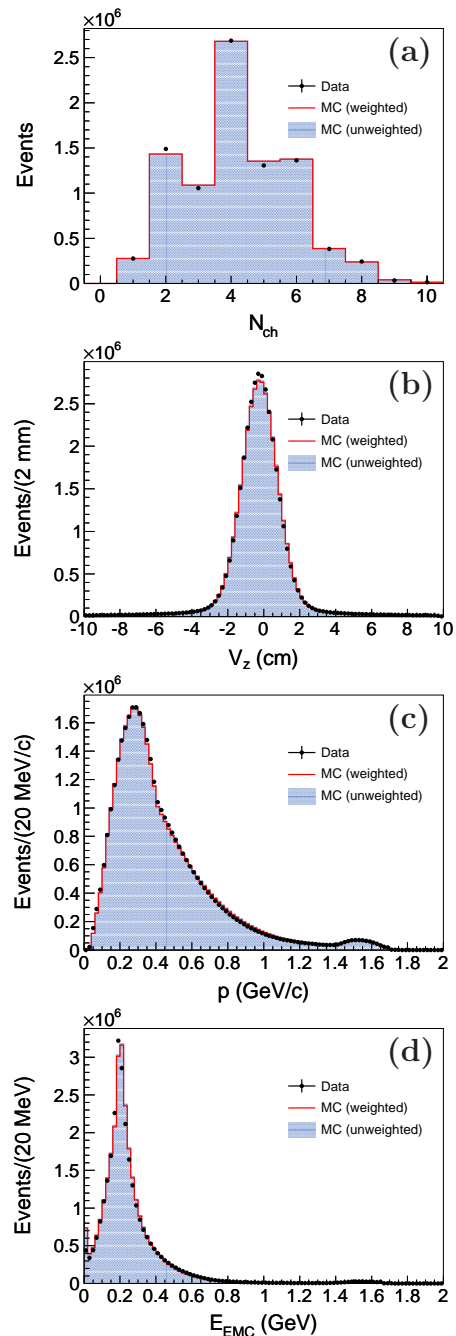


FIG. 1. The distributions are (a) N_{ch} , (b) V_z , (c) p , and (d) E_{EMC} . Data are represented by dots, and the MC sample by the red and shaded histograms for the weighted and unweighted MC events, respectively.

event, or a $\pi^0\pi^0J/\psi$ event. The $\pi^+\pi^-J/\psi$ events are selected with the following requirements. There are two oppositely charged pions with momenta $p_\pi < 0.45$ GeV/ c , and the mass recoiling from the $\pi^+\pi^-$ system, RM^{+-} , must satisfy $3.09 < RM^{+-} < 3.11$ GeV/ c^2 . The $\pi^0\pi^0J/\psi$ events must have two π^0 s with $p_\pi < 0.45$ GeV/ c , and the mass recoiling from the $\pi^0\pi^0$ system, RM^{00} , must satisfy $3.085 < RM^{00} < 3.12$ GeV/ c^2 .

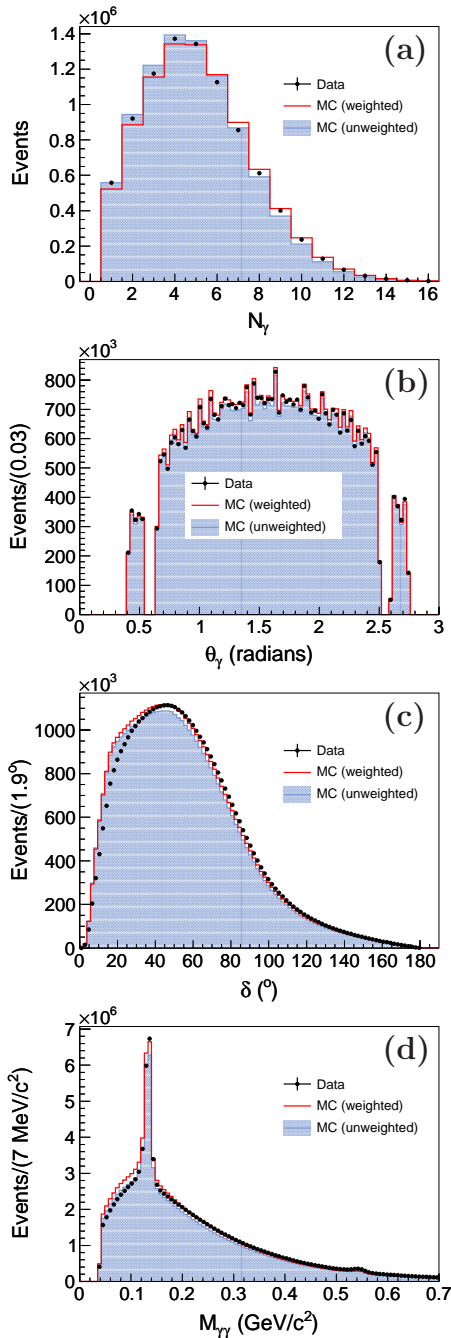


FIG. 2. The distributions are (a) N_γ , (b) θ_γ , (c) δ , and (d) $M_{\gamma\gamma}$ of all $\gamma\gamma$ combinations. Here θ_γ is the polar angle of the photon. Data are represented by dots, and the MC sample by the red and shaded histograms for the weighted and unweighted MC events, respectively.

The photon must be in the EMC barrel. This requirement is used because the energy resolution is better for barrel photons, and there are fewer noise photons. The photon must satisfy the requirement of $\delta < 14$ degrees (see Section III C) and not be part of a π^0 candidate. In Fig. 4 (a) and (b), inclusive photon energy distributions after the above selection requirements are

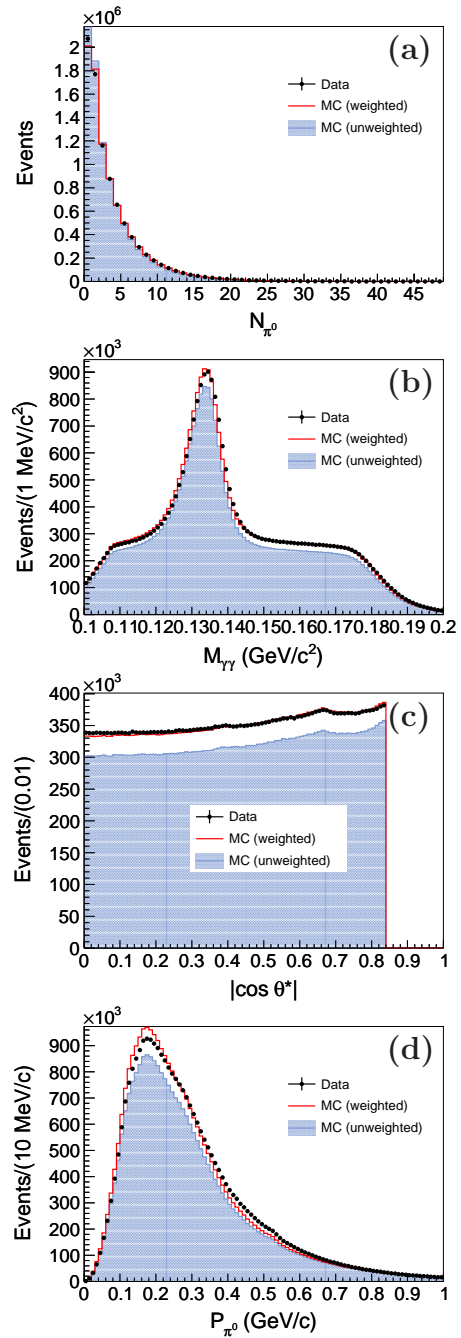


FIG. 3. The distributions of π^0 candidates are (a) N_{π^0} , (b) $M_{\gamma\gamma}$ made without the π^0 mass selection requirement, (c) $|\cos \theta^*|$, (d) p_{π^0} . Data are represented by dots, and the MC sample by the red and shaded histograms for the weighted and unweighted MC events, respectively.

shown for data and inclusive MC events, respectively. The peaks from left to right in each distribution correspond to $\psi(3686) \rightarrow \gamma\chi_{c2}, \gamma\chi_{c1}, \gamma\chi_{c0}, \chi_{c1} \rightarrow \gamma J/\psi$, and $\chi_{c2} \rightarrow \gamma J/\psi$. The very small peak at around 0.65 GeV is from the $\psi(3686) \rightarrow \gamma\eta_c$ transition. Other small peaks not seen in the spectra but considered in the fit are $J/\psi \rightarrow \gamma\eta_c$ and $\chi_{c0} \rightarrow \gamma J/\psi$.

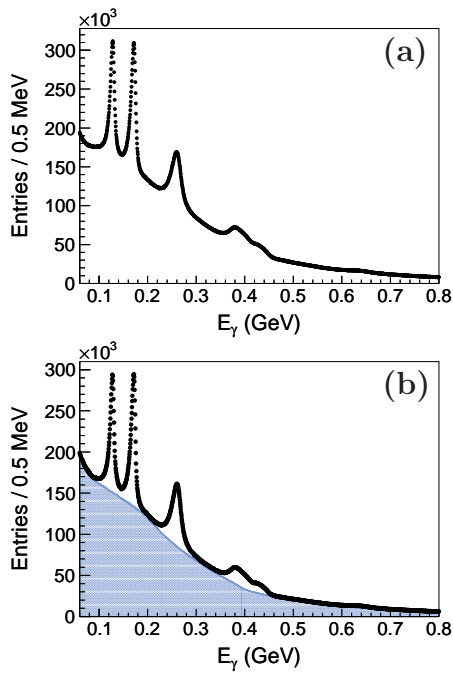


FIG. 4. Inclusive photon energy distributions for (a) data and (b) inclusive MC events, where the shaded region in (b) has the radiative photons removed. Peaks from left to right are $\psi(3686) \rightarrow \gamma\chi_{c2}$, $\gamma\chi_{c1}$, $\gamma\chi_{c0}$ and χ_{c1} and $\chi_{c2} \rightarrow \gamma J/\psi$. The $\chi_{c0} \rightarrow \gamma J/\psi$ peak is not visible. The very small peak around 0.65 GeV is $\psi(3686) \rightarrow \gamma\eta_c$.

The inclusive $\psi(3686)$ MC sample is used to obtain the signal shapes for charmonium transitions and the shape of the major component of the background under the signal peaks. The signal shape for each transition is obtained by matching the radiative photon at the generator level with one of the photons reconstructed in the EMC. The requirement, which has an efficiency greater than 99%, is that the angle between the radiative photon and the reconstructed photon in the EMC must be less than 0.08 radians. No requirement on the energy is used to allow obtaining the tails of the energy distribution. The signal shapes are shown in Fig. 5. The three large peaks from left to right in Fig. 5 (a) correspond to the $\psi(3686) \rightarrow \gamma\chi_{c2}$, $\gamma\chi_{c1}$, and $\gamma\chi_{c0}$ transitions. The very small peak around 0.65 GeV is the $\psi(3686) \rightarrow \gamma\eta_c$ transition. The peaks in Fig. 5 (b) from left to right correspond to the $\chi_{cJ} \rightarrow \gamma J/\psi$ transitions for $J = 0, 1$, and 2, where the $\chi_{c0} \rightarrow \gamma J/\psi$ peak at around 0.3 GeV is very small.

The background component is obtained from the simulated inclusive photon energy distribution after all selection requirements but with energy deposits from radiative photons for charmonium radiative transition events ($\psi(3686) \rightarrow \gamma\chi_{cJ}$, $\psi(3686) \rightarrow \gamma\eta_c$, $\chi_{cJ} \rightarrow \gamma J/\psi$, and $J/\psi \rightarrow \gamma\eta_c$) removed. Note that this distribution, shown as the shaded region in Fig. 4 (b), has a complicated shape. This distribution will be used to describe part of the background under the signal peaks in fitting the

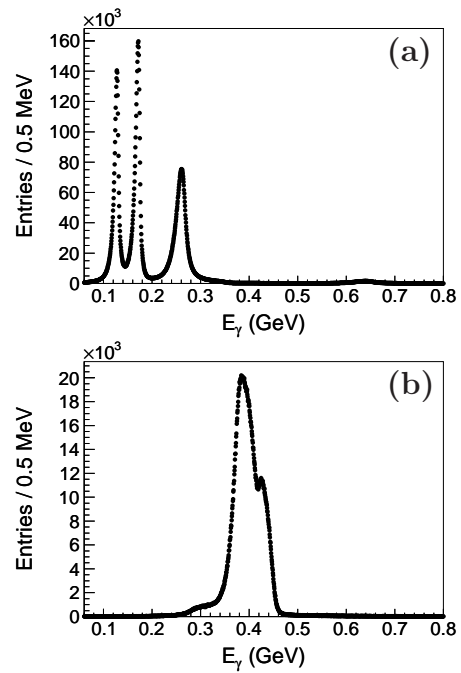


FIG. 5. Photon energy line shapes from inclusive MC. (a) Peaks from left to right are $\psi(3686) \rightarrow \gamma\chi_{c2}$, $\gamma\chi_{c1}$, and $\gamma\chi_{c0}$. (b) Peaks from left to right are χ_{c0} , χ_{c1} , and $\chi_{c2} \rightarrow \gamma J/\psi$.

data and MC inclusive photon energy distributions, as described in Section VI.

The $E1$ transition is expected to have an energy dependence of E_γ^3 , where E_γ is the energy of the radiative photon in the CM of the parent particle [29]. To account for the $E1$ transitions for $\psi(3686) \rightarrow \gamma\chi_{cJ}$, $\chi_{cJ} \rightarrow \gamma J/\psi$, a weight (w_{trans}) is calculated for each MC event using the radiative photon CM energy. For $\psi(3686) \rightarrow \gamma_1\chi_{cJ}$ events with no subsequent $\chi_{cJ} \rightarrow \gamma J/\psi$ decay, the weights are given by $(\frac{E_{\gamma_1}}{E_{\gamma_{10}}})^3$, where E_{γ_1} for each decay is the radiative photon CM energy and $E_{\gamma_{10}}$ is the most probable transition energy ($E_{\gamma_{10}} = \frac{E_{\text{cm}}^2 - M_{\chi_{cJ}}^2}{2 \times E_{\text{cm}}}$). For $\psi(3686) \rightarrow \gamma_1\chi_{cJ}$, $\chi_{cJ} \rightarrow \gamma_2 J/\psi$ events, the weights are calculated according to $(\frac{E_{\gamma_1}}{E_{\gamma_{10}}})^3 (\frac{E_{\gamma_2}}{E_{\gamma_{20}}})^3$, where E_{γ_2} is the energy of the daughter radiative photon in the rest frame of the mother particle and $E_{\gamma_{20}}$ is its most probable energy. The overall event weight is the product of both weights ($w_{\pi^0} \times w_{\text{trans}}$).

V. $\psi(3686) \rightarrow \gamma\chi_{cJ}$ EXCLUSIVE EVENT SELECTION AND PHOTON ENERGY DISTRIBUTIONS

In order to constrain the final $\psi(3686) \rightarrow \gamma\chi_{cJ}$ signal shapes in fitting inclusive photon energy distributions, clean energy spectra from $\psi(3686) \rightarrow \gamma\chi_{cJ}$, $\chi_{cJ} \rightarrow \text{exclusive events}$ will be used. To fit the $\psi(3686) \rightarrow \gamma\chi_{cJ}$ peaks of data, exclusive event samples are selected from

$\psi(3686)$ data. To fit the MC $\psi(3686) \rightarrow \gamma\chi_{cJ}$ peaks, exclusive samples are generated, as described below. Exclusive events must satisfy the same requirements as inclusive events when constructing photon energy distributions.

A. $\psi(3686) \rightarrow \gamma\chi_{cJ}$ exclusive event selection

The exclusive $\psi(3686) \rightarrow \gamma\chi_{cJ}$ photon energy distribution is the sum of $\psi(3686) \rightarrow \gamma\chi_{cJ}, \chi_{cJ} \rightarrow 2$ and 4 charged track events.

Common requirements The number of good photons must be greater than zero and less than 17. The photon with the minimum θ_{recoil} , which is the angle between the photon and the momentum recoiling from the two (four) charged tracks, is selected as the radiative photon, and θ_{recoil} must satisfy $\theta_{recoil} < 0.2$ rad. Also required are $|\cos\theta_{rad-\gamma}| < 0.75$, where $\theta_{rad-\gamma}$ is the polar angle of the radiative photon, and $3.3 < M_{2(4)\pi} < 3.62$ GeV/ c^2 , where $M_{2(4)\pi}$ is the invariant mass of the two (four) charged tracks.

Specific requirements for $\psi(3686) \rightarrow \gamma\chi_{cJ}, \chi_{cJ} \rightarrow 2$ charged tracks We require one positively and one negatively charged track. Particle identification probabilities are determined using dE/dx information from the MDC and time of flight information from the TOF system, and both tracks are required to be either kaons ($\text{Prob}(K) > \text{Prob}(\pi)$) or pions ($\text{Prob}(\pi) > \text{Prob}(K)$). We also require $|\cos\theta| < 0.85$ for both charged tracks, where θ is the polar angle, the momentum of each track be less than 1.4 GeV/ c , and the momentum of one track be larger than 0.5 GeV/ c .

Specific requirements for $\psi(3686) \rightarrow \gamma\chi_{cJ}, \chi_{cJ} \rightarrow 4$ charged tracks We require two positive and two negative tracks and $|\Sigma p_z| < 0.04$ GeV/ c , where $|\Sigma p_z|$ is the sum of the momenta of the charged tracks and neutral clusters in the z direction. ISR events tend to have large $|\Sigma p_z|$. Also the mass recoiling from the two low momentum tracks is required to be less than 3.05 GeV/ c^2 to veto $\psi(3686) \rightarrow \pi\pi J/\psi$ background.

B. $\psi(3686) \rightarrow \gamma\chi_{cJ}$ exclusive MC sample

Here, exclusive $\chi_{cJ} \rightarrow$ two and four pion and kaon events are generated with EVTGEN [25], and the generated events are selected using the selection criteria described in Section V A. Events are weighted by w_{trans} using the generated energy of the radiative photon.

VI. FITTING THE INCLUSIVE PHOTON ENERGY DISTRIBUTION

The numbers of $\psi(3686) \rightarrow \gamma\chi_{cJ}$ events and $\chi_{cJ} \rightarrow \gamma J/\psi$ events are obtained by fitting the inclusive photon

energy distributions for data. The efficiencies are obtained from the fit results for the inclusive $\psi(3686)$ MC events.

To fit the $\psi(3686) \rightarrow \gamma\chi_{cJ}$ signal peaks of data, the MC signal shapes, described in Section IV, are convolved with asymmetric Gaussians to account for the difference in resolution between MC and data, where the parameters of the Gaussians are determined by the fit. The broad χ_{c1} and $\chi_{c2} \rightarrow \gamma J/\psi$ peaks are described well by just the MC shapes. Also included in the fit are $\chi_{c0} \rightarrow \gamma J/\psi$ and $J/\psi \rightarrow \gamma\eta_c$. The background distribution is the inclusive MC photon energy distribution with energy deposits from radiative photons removed combined with a second order Chebychev polynomial function.

To constrain further the $\psi(3686) \rightarrow \gamma\chi_{cJ}$ signal shapes, a simultaneous fit to inclusive (see Section IV) and exclusive photon energy distributions (see Section V A) is done in the energy range from 0.08 to 0.35 GeV. The parameters of the asymmetric Gaussians are the same for the inclusive and exclusive fits. However, all signal shapes are allowed to shift independently in energy for the two distributions. The exclusive background distribution is determined in a similar way as the inclusive photon background distribution but using the exclusive event selection on the $\psi(3686)$ MC event sample.

Shown in Fig. 6 is the simultaneous fit of data for the region $0.08 < E_\gamma < 0.5$ GeV for the inclusive photon energy distribution and the region $0.08 < E_\gamma < 0.35$ GeV for the exclusive photon energy distribution. The fit to the inclusive photon energy distribution and the corresponding pull distribution are shown in the top set of plots. The bottom set of plots are those for the exclusive photon energy distribution. The pull distributions are reasonable, except in the vicinity of the $\psi(3686) \rightarrow \gamma\chi_{c1}$ and $\gamma\chi_{c2}$ peaks. The chi-squares per degree of freedom (ndf) are 3.5 and 2.7 for the inclusive and exclusive distribution fits, respectively. The chi-square is determined using $\chi^2 = \Sigma_i ((n_i - n_i^f)/\sigma_i)^2$, where n_i , n_i^f , and σ_i are the number of data events in bin i , the result of the fit at bin i , and the statistical uncertainty of n_i , respectively, and the sum is over all histogram bins.

A fit is also done to the MC inclusive energy distribution. The MC shapes are used without convolved asymmetric Gaussians for the $\psi(3686) \rightarrow \gamma\chi_{cJ}$ peaks. Since only MC shapes are used, it is not useful to do a simultaneous fit as there are no common parameters to be determined in such a fit. The fit matches the inclusive photon energy distribution almost perfectly with a chisquare close to zero. This is not unexpected since the signal and background shapes come from the MC and when combined reconstruct the MC distribution.

TABLE II. Branching fraction results. The indicated uncertainties are statistical only.

Branching Fraction	Events ($\times 10^6$)	Efficiency	Branching Fraction (%)
$\mathcal{B}(\psi(3686) \rightarrow \gamma\chi_{c0})$	4.6871 ± 0.0068	0.4692	9.389 ± 0.014
$\mathcal{B}(\psi(3686) \rightarrow \gamma\chi_{c1})$	4.9957 ± 0.0054	0.4740	9.905 ± 0.011
$\mathcal{B}(\psi(3686) \rightarrow \gamma\chi_{c2})$	4.2021 ± 0.0055	0.4104	9.621 ± 0.013
$\mathcal{B}(\psi(3686) \rightarrow \gamma\chi_{c0}) \times \mathcal{B}(\chi_{c0} \rightarrow \gamma J/\psi)$	0.0123 ± 0.0081	0.4920	0.024 ± 0.015
$\mathcal{B}(\psi(3686) \rightarrow \gamma\chi_{c1}) \times \mathcal{B}(\chi_{c1} \rightarrow \gamma J/\psi)$	1.8881 ± 0.0053	0.5155	3.442 ± 0.010
$\mathcal{B}(\psi(3686) \rightarrow \gamma\chi_{c2}) \times \mathcal{B}(\chi_{c2} \rightarrow \gamma J/\psi)$	0.9828 ± 0.0041	0.5150	1.793 ± 0.008
$\mathcal{B}(\chi_{c0} \rightarrow \gamma J/\psi)$			0.25 ± 0.16
$\mathcal{B}(\chi_{c1} \rightarrow \gamma J/\psi)$			34.75 ± 0.11
$\mathcal{B}(\chi_{c2} \rightarrow \gamma J/\psi)$			18.64 ± 0.08

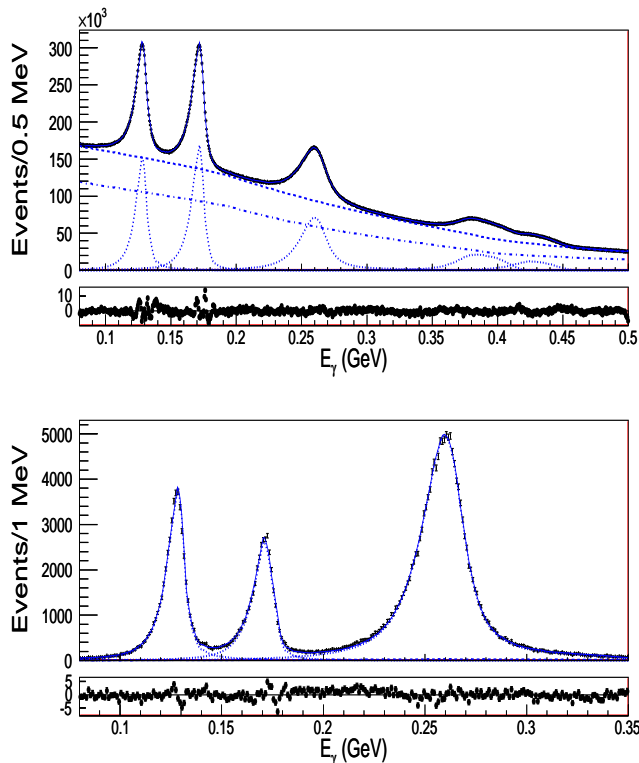


FIG. 6. Simultaneous fits to the photon energy distributions of data. (Top set) Inclusive distribution fit and corresponding pulls, and (Bottom set) exclusive distribution fit and pull distribution. Peaks from left to right in the top set are $\psi(3686) \rightarrow \gamma\chi_{c2}$, $\gamma\chi_{c1}$, and $\gamma\chi_{c0}$ and χ_{c1} and $\chi_{c2} \rightarrow \gamma J/\psi$. The $\chi_{c0} \rightarrow \gamma J/\psi$ peak is not visible. The smooth curves in the two plots are the fit results. The dashed-dotted and dashed curves in the top plot are the background distribution from the inclusive $\psi(3686)$ MC with radiative photons removed and the total background, respectively. The background in the exclusive fit plot is not visible.

VII. BRANCHING FRACTION DETERMINATIONS

The branching fractions are calculated using the following equations

$$\mathcal{B}(\psi(3686) \rightarrow \gamma\chi_{cJ}) = \frac{N_{\psi(3686) \rightarrow \gamma\chi_{cJ}}}{\epsilon_{\psi(3686) \rightarrow \gamma\chi_{cJ}} \times N_{\psi(3686)}}, \quad (1)$$

where $\mathcal{B}(\psi(3686) \rightarrow \gamma\chi_{cJ})$ is the branching fraction of $\psi(3686) \rightarrow \gamma\chi_{cJ}$, $N_{\psi(3686) \rightarrow \gamma\chi_{cJ}}$ is the number of events in data from the fit, $\epsilon_{\psi(3686) \rightarrow \gamma\chi_{cJ}}$ is the efficiency determined from MC, and $N_{\psi(3686)}$ is the number of $\psi(3686)$ events [17]. The product branching fraction for $\psi(3686) \rightarrow \gamma\chi_{cJ}$, $\chi_{cJ} \rightarrow \gamma J/\psi$ is given by

$$\begin{aligned} \mathcal{B}(\psi(3686) \rightarrow \gamma\chi_{cJ}) \times \mathcal{B}(\chi_{cJ} \rightarrow \gamma J/\psi) \\ = \frac{N_{\chi_{cJ} \rightarrow \gamma J/\psi}}{\epsilon_{\chi_{cJ} \rightarrow \gamma J/\psi} \times N_{\psi(3686)}}, \end{aligned} \quad (2)$$

where $N_{\chi_{cJ} \rightarrow \gamma J/\psi}$ is the number of $\chi_{cJ} \rightarrow \gamma J/\psi$ events in data and $\epsilon_{\chi_{cJ} \rightarrow \gamma J/\psi}$ is the efficiency. From Eq. (1) and Eq. (2), we obtain the branching fraction for $\chi_{cJ} \rightarrow \gamma J/\psi$, which is given by

$$\begin{aligned} \mathcal{B}(\chi_{cJ} \rightarrow \gamma J/\psi) \\ = \frac{\mathcal{B}(\psi(3686) \rightarrow \gamma\chi_{cJ}) \times \mathcal{B}(\chi_{cJ} \rightarrow \gamma J/\psi)}{\mathcal{B}(\psi(3686) \rightarrow \gamma\chi_{cJ})} \\ = \frac{\epsilon_{\psi(3686) \rightarrow \gamma\chi_{cJ}} \times N_{\chi_{cJ} \rightarrow \gamma J/\psi}}{\epsilon_{\chi_{cJ} \rightarrow \gamma J/\psi} \times N_{\psi(3686) \rightarrow \gamma\chi_{cJ}}}. \end{aligned} \quad (3)$$

Results are listed in Table II, where the uncertainties are statistical only. For $\mathcal{B}(\chi_{cJ} \rightarrow \gamma J/\psi)$, an alternative parametrization in terms of $N_{\psi(3686) \rightarrow \gamma\chi_{cJ}}$ and the ratio $N_{\chi_{cJ} \rightarrow \gamma J/\psi}/N_{\psi(3686) \rightarrow \gamma\chi_{cJ}}$ has been tried because of the possible correlation between the numerator and denominator of Eq. (3), but the difference with the original result is small and will be neglected since it is much less than the systematic uncertainties that will be discussed below.

VIII. SYSTEMATIC UNCERTAINTIES

Systematic uncertainties, which arise from selection requirements, fitting, photon efficiency, the uncertainty in the number of $\psi(3686)$ events, etc. are summarized in Table III. For $\psi(3686) \rightarrow \gamma\chi_{cJ}$, they are under 4% and smaller than those of CLEO [9], with the largest contribution coming from fitting the photon energy distribution. Details of how they are estimated are given below.

A. Systematic uncertainties from initial $\psi(3686)$ event selection

Initial $\psi(3686)$ event selection requirements are $N_{\text{ch}} > 0$, $N_\gamma < 17$, and $E_{\text{vis}} > 0.22E_{\text{cm}}$. To determine the systematic uncertainties associated with the $N_{\text{ch}} > 0$ requirement, events without charged tracks are also analyzed. The photon time requirement is removed for these events since without charged tracks, the event start time can not be well determined. The selection requirements are also changed because these events have much more background. Events must have total energy greater than 1.7 GeV and at least one good neutral pion. Even so, there is a background from low energy photons, and even after subtracting continuum, the photon energy distribution for data has a large background under the signal peaks, making fits difficult with the number of fitted events having large uncertainties.

The photon energy distributions for data and MC are fitted. The numbers of fitted events for data and MC are then added with the number of fitted events with charged tracks, and the branching fractions are recalculated. The differences with the branching fractions determined with charged track events only are then determined and taken as the systematic uncertainties associated with the $N_{\text{ch}} > 0$ requirement.

As described in Section III D, inclusive $\psi(3686)$ MC events are weighted according to the N_{π^0} distribution to give better agreement with data. According to the MC, the efficiency of the $N_\gamma < 17$ requirement, defined as the number of events with $N_\gamma < 17$ divided by the number of events with $N_\gamma > 0$, is 99.99% with weighting and 99.99% without weighting, while the efficiency for data is 99.98%. The agreement is excellent, the efficiency is very high, and the systematic uncertainty is negligible for this requirement.

The agreement between the E_{vis} distribution of data and the inclusive $\psi(3686)$ MC distribution is very good. According to the inclusive MC, the efficiency of the $E_{\text{vis}} > 0.22E_{\text{cm}}$ requirement after the N_{ch} and N_γ requirements is 99.76%. The mean and root-mean-squared values of the MC (data) are 3.004 (2.991) GeV and 0.561 (0.579) GeV, respectively. If the MC distribution is shifted down by 13 MeV relative to the data, the loss of events due to the E_{vis} requirement corresponds to an inefficiency of 0.17%, and this will be taken as the systematic uncertainty for the E_{vis} requirement.

B. Systematic uncertainties from inclusive photon selection

Further selection criteria are used before including photons into the photon energy distributions which are used for fitting. Photon selection requirements include $\delta > 14^\circ$, removal of non- $\psi(3686)$ background events, removal of $\pi\pi J/\psi$ events, and removal of photons which can be part of a π^0 .

$\delta > 14^\circ$ and $\psi(3686)$ background removal systematic uncertainties:

To determine the systematic uncertainties for the first two requirements, they are removed from the selection process, and the branching fraction results obtained are compared to those with the requirements. Removing the δ requirement changes the inclusive photon energy background distribution of the inclusive MC, as well as the inclusive photon energy distribution of data. The differences of the branching fraction results are taken as the systematic uncertainties for each of the requirements.

$\pi^+\pi^- J/\psi$ event removal systematic uncertainty:

The distribution of mass recoiling from the $\pi^+\pi^-$ system, RM^{+-} , for events passing the non- $\psi(3686)$ veto and the $\psi(3686) \rightarrow \pi^+\pi^- J/\psi$ selection, but without the recoil mass requirement in Section IV, has a clear J/ψ peak from $\psi(3686) \rightarrow \pi^+\pi^- J/\psi$. Events with RM^{+-} satisfying $3.09 < RM^{+-} < 3.11$ GeV/ c^2 will be removed from further consideration. However, there are $\pi^+\pi^-$ mis-combinations underneath the peak in the J/ψ region. To estimate the probability that a good radiative photon event may be vetoed accidentally (or the efficiency with which it will pass this veto requirement), the sideband regions, defined as $3.07 < RM^{+-} < 3.085$ GeV/ c^2 and $3.115 < RM^{+-} < 3.13$ GeV/ c^2 , are used to estimate the number of mis-combinations in the signal region. Using this veto probability, the efficiency for inclusive MC events to pass the $\psi(3686) \rightarrow \pi^+\pi^- J/\psi$ veto requirement is found to be 93.06%. The efficiency for data is 92.83%, and the difference between data and inclusive MC is $0.23/93.06 = 0.25\%$, which we take as the systematic uncertainty due to the $\pi^+\pi^- J/\psi$ veto for all radiative photon processes.

$\pi^0\pi^0 J/\psi$ event removal systematic uncertainty:

The approach to determine the systematic uncertainty for the $\pi^0\pi^0 J/\psi$ event removal is similar to that described in the previous section. Using the veto probability obtained using sidebands, the efficiency for inclusive MC events to pass the $\psi(3686) \rightarrow \pi^0\pi^0 J/\psi$ veto requirement is found to be 95.34%. The efficiency for data is 95.37%, and the difference between data and inclusive MC is $0.03/95.35 = 0.03\%$, which we will take as the systematic uncertainty due to the $\pi^0\pi^0 J/\psi$ veto for all radiative photon processes.

Systematic uncertainty for the removal of photons which can be part of a π^0 :

As described in Section III C, photons that are part of a π^0 are excluded from the inclusive photon energy distri-

TABLE III. Relative systematic uncertainties (%). $\mathcal{B}_{\psi J}$ is notation for $\mathcal{B}(\psi(3686) \rightarrow \gamma\chi_{cJ})$, \mathcal{B}_{PJ} is for $\mathcal{B}(\psi(3686) \rightarrow \gamma\chi_{cJ}) \times \mathcal{B}(\chi_{cJ} \rightarrow \gamma J/\psi)$, and $\mathcal{B}_{\chi J}$ is for $\mathcal{B}(\chi_{cJ} \rightarrow \gamma J/\psi)$. Some uncertainties cancel in the determination of $\mathcal{B}_{\chi 1}$ and $\mathcal{B}_{\chi 2}$ and are left blank in the table. Since the fit uncertainty is so large for $\psi(3686) \rightarrow \gamma\chi_{c0}, \chi_{c0} \rightarrow \gamma J/\psi$, the other systematic uncertainties for \mathcal{B}_{P0} and $\mathcal{B}_{\chi 0}$ are omitted.

	$\mathcal{B}_{\psi 0}$	$\mathcal{B}_{\psi 1}$	$\mathcal{B}_{\psi 2}$	\mathcal{B}_{P0}	\mathcal{B}_{P1}	\mathcal{B}_{P2}	$\mathcal{B}_{\chi 0}$	$\mathcal{B}_{\chi 1}$	$\mathcal{B}_{\chi 2}$
$N_{\text{ch}} > 0$	0.74	0.27	0.75		0.06	0.74		0.21	1.5
$N_{\gamma} < 17$	-	-	-		-	-			
$E_{\text{vis}} > 0.22E_{\text{cm}}$	0.17	0.17	0.17		0.17	0.17			
$\delta > 14^\circ$	0.36	0.14	0.00		0.02	1.56		0.12	1.42
$\psi(3686)$ background veto	0.51	0.73	0.15		0.51	0.11		1.25	0.26
$\pi^+\pi^- J/\psi$ veto	0.25	0.25	0.25		0.25	0.25			
$\pi^0\pi^0 J/\psi$ veto	0.03	0.03	0.03		0.03	0.03			
γ not in π^0	0.87	0.53	0.19		1.24	2.3		1.35	2.3
Fitting	2.62	2.69	1.5	869	3.10	7.22	861	4.43	7.27
MC signal shape	0.06	0.17	0.53		0.07	0.53		0.24	1.05
Multipole correction	0.0	0.61	0.60		0.35	3.82		0.70	3.87
$ \cos\theta < 0.8$	0.49	0.12	0.07		0.35	1.46		0.47	1.52
π^0 weight	1.19	1.55	1.60		1.09	1.73		0.47	0.13
Continuum energy difference	0.75	0.06	0.43		0.35	0.60		0.39	1.02
γ efficiency	1.0	1.0	1.0		1.0	1.0			
$N_{\psi(3686)}$	0.81	0.81	0.81		0.81	0.81			
Total	3.54	3.57	2.83	869	3.84	9.09	861	4.92	9.05

bution. To estimate the systematic uncertainty for this requirement, the efficiency of this criterion is determined for data and MC events for each transition by fitting the photon inclusive energy distribution with and without the π^0 removal using non-simultaneous fitting. The systematic uncertainties are determined by the differences between the efficiencies for data and MC events.

C. Fitting systematic uncertainty

The systematic uncertainty associated with the fit procedure is determined by comparing various fitting methods. The fit is done with an alternative strategy, fitting with a non-simultaneous fit, changing the order of the polynomial function used from second order to first order, changing the fitting range, and fixing the number of events for the $J/\psi \rightarrow \gamma\eta_c$ and $\psi(3686) \rightarrow \gamma\chi_{c0}, \chi_{c0} \rightarrow \gamma J/\psi$ to the numbers expected, and the result for each case is compared with our standard fit to determine the systematic uncertainty for that case.

For the alternative strategy, the $\psi(3686) \rightarrow \gamma\chi_{c1}$ and $\gamma\chi_{c2}$ peaks are described by asymmetric Gaussians with Crystal Ball tails on both sides. The other signal peaks and backgrounds are the same. A simultaneous fit is done to better constrain the asymmetric Gaussian and Crystal Ball tail parameters, which are common between the inclusive and exclusive distributions.

For the $\psi(3686) \rightarrow \gamma\chi_{cJ}$ systematic uncertainties, the fitting range is changed from 0.08 – 0.5 GeV to 0.08 – 0.35 GeV, which removes the $\chi_{cJ} \rightarrow \gamma J/\psi$ peaks and changes the number of parameters used in the fit. For the $\chi_{cJ} \rightarrow \gamma J/\psi$ systematic uncertainties, the range is

changed from 0.08 – 0.5 GeV to 0.2 – 0.54 GeV, which removes the $\psi(3686) \rightarrow \gamma\chi_{c1}$ and $\psi(3686) \rightarrow \gamma\chi_{c2}$ peaks and produces a rather large systematic uncertainty due to the background in the fit of data preferring a pure polynomial background in the latter case. The total systematic uncertainties from fitting for each branching fraction are determined by adding the systematic uncertainties from each source in quadrature.

The signal for $\psi(3686) \rightarrow \gamma\chi_{c0}, \chi_{c0} \rightarrow \gamma J/\psi$ is very small and sits on the tail of $\psi(3686) \rightarrow \gamma\chi_{c0}$. It is therefore difficult to fit this peak as indicated by the very large fitting systematic uncertainty for this process.

D. MC Signal Shape

The signal shapes used in fitting the photon energy distribution are determined by matching MC radiative photons with reconstructed photons in the EMC, where the angle between the photons is required to be less than $\Delta\theta = 0.08$ radians. This selection could bias the signal shapes used in the fitting. The systematic uncertainty associated with this selection is determined by changing the $\Delta\theta$ selection requirement to 0.04 radians. The differences for each decay are taken as the systematic uncertainties in the signal shape.

E. Higher order multipoles for $\psi(3686) \rightarrow \gamma\chi_{c1}$ and χ_{c2}

Angular distributions for $\psi(3686) \rightarrow \gamma\chi_{cJ}$ are generated according to those expected for $E1$ radiative tran-

sitions. This approach is accurate enough for $\psi(3686) \rightarrow \gamma\chi_{c0}$, but higher order multipole contributions must be considered for $\psi(3686) \rightarrow \gamma\chi_{c1}$ and $\psi(3686) \rightarrow \gamma\chi_{c2}$ decays. Also the angular distributions for $\chi_{cJ} \rightarrow \gamma J/\psi$ MC events do not agree with data. BESIII has measured the angular distributions for $\psi(3686) \rightarrow \gamma\chi_{cJ}, \chi_{cJ} \rightarrow \gamma J/\psi$ [16], and these distributions have been fitted to $1 + \alpha \cos^2 \theta$, where θ is the laboratory polar angle, and the values of α have been determined. Using these values of α , it is possible to calculate the differences in the geometric acceptance between data and the inclusive $\psi(3686)$ MC. The acceptance efficiency for a given value of α is given by the integral of $1 + \alpha \cos^2 \theta$ from $\cos \theta = -0.8$ to $\cos \theta = 0.8$ divided by the integral between -1 and $+1$. Using the values of α that were used to generate the MC events and those obtained based on Ref. [16], the changes in the efficiencies are 0.61% for $\psi(3686) \rightarrow \gamma\chi_{c1}$ and 0.60% for $\psi(3686) \rightarrow \gamma\chi_{c2}$. For $\chi_{cJ} \rightarrow \gamma J/\psi$ ($J = 1, 2$), the changes are 0.35% and 3.82%, respectively. The changes to the branching fractions from the changes in efficiencies are taken as the systematic uncertainties due to the higher order multipole corrections.

F. $|\cos \theta| < 0.8$

The systematic uncertainty associated with the $|\cos \theta| < 0.8$ requirement is determined by using the requirement $|\cos \theta| < 0.75$ instead and by comparing the results with the standard requirement. This tests whether there are edge effects with the EMC that are not fully modeled by the MC simulations.

G. Event weighting

As described in Section III D, MC events are weighted to give better agreement for the π^0 distributions between data and MC simulation, as well as to include the $E1$ transition E_γ^3 weight. The systematic uncertainty associated with the w_{π^0} weight is determined by turning off its weighting and taking the difference in results as the systematic uncertainties.

H. Continuum energy difference

Data distributions, including the inclusive photon energy distribution for data, are defined as data minus scaled continuum data. While this takes into consideration the effect on the normalization of the continuum due to the difference in luminosity and energy, it does not consider the difference in the energy scale of the photons. To determine the systematic uncertainty due to this effect, the photon energies of the continuum data were scaled by the ratio of the CM energies, $3.686/3.65$, and the scaled distribution was subtracted from data, and the fitting redone. The differences with respect to

the standard analysis are taken as the systematic uncertainties of this effect.

I. Other systematic uncertainties

The photon detection efficiency is studied utilizing the control samples $\psi(3686) \rightarrow \pi^+\pi^- J/\psi, J/\psi \rightarrow \rho^0\pi^0$ and $\psi(3686) \rightarrow \pi^0\pi^0 J/\psi$ with $J/\psi \rightarrow l^+l^-$ and $\rho^0\pi^0$. The corresponding systematic uncertainty is estimated by the difference of detection efficiency between data and MC samples, and 1% is assigned for each photon [30].

The trigger efficiency is assumed to be very close to 100% with negligible uncertainty, since the average charged particle and photon multiplicities are high. The number of $\psi(3686)$ events is $(106.41 \pm 0.86) \times 10^6$, which is obtained by studying inclusive $\psi(3686)$ decays [17]. The uncertainties from all above sources and the total systematic uncertainty, obtained by adding all uncertainties quadratically, are listed in Table III. Since the fitting uncertainty for $\psi(3686) \rightarrow \gamma\chi_{c0}, \chi_{c0} \rightarrow \gamma J/\psi$ is so large, indicating that this fit is not very meaningful, only this uncertainty is listed in the table.

IX. RESULTS

Our results are listed in Table IV. We also calculate ratios of branching fractions, where common systematic uncertainties cancel

$$\begin{aligned} \mathcal{B}(\psi(3686) \rightarrow \gamma\chi_{c0})/\mathcal{B}(\psi(3686) \rightarrow \gamma\chi_{c1}) &= 0.948 \pm 0.002 \pm 0.044 \\ \mathcal{B}(\psi(3686) \rightarrow \gamma\chi_{c0})/\mathcal{B}(\psi(3686) \rightarrow \gamma\chi_{c2}) &= 0.976 \pm 0.002 \pm 0.040 \\ \mathcal{B}(\psi(3686) \rightarrow \gamma\chi_{c2})/\mathcal{B}(\psi(3686) \rightarrow \gamma\chi_{c1}) &= 0.971 \pm 0.002 \pm 0.040 \end{aligned}$$

For comparison with some theoretical calculations, we also determine partial widths using our branching fractions and the world average full widths [7]. Table V contains our partial width results, as well as theoretical predictions, reproduced from Table VI in Ref. [8]. The theoretical predictions include the linear potential (LP) and screened potential (SP) models [8], as well as earlier predictions from a relativistic quark model (RQM) [33], non-relativistic potential and Godfrey-Isgur relativized potential models (NR/GI) [34], and color screened models, calculated with zeroth order wave functions (SNR₀) and first order relativistically corrected wave functions (SNR₁) [35].

X. SUMMARY

Our results, CLEO measurements [9, 31, 32], previous BESIII measurements [15, 16], and PDG results [7]

TABLE IV. Our branching fraction results, other results, and PDG compilation results.

Branching Fraction	This analysis (%)	Other (%)	PDG [7] (%) Average	PDG [7] (%) Fit
$\mathcal{B}(\psi(3686) \rightarrow \gamma\chi_{c0})$	$9.389 \pm 0.014 \pm 0.332$	$9.22 \pm 0.11 \pm 0.46$ [9]	9.2 ± 0.4	9.99 ± 0.27
$\mathcal{B}(\psi(3686) \rightarrow \gamma\chi_{c1})$	$9.905 \pm 0.011 \pm 0.353$	$9.07 \pm 0.11 \pm 0.54$ [9]	8.9 ± 0.5	9.55 ± 0.31
$\mathcal{B}(\psi(3686) \rightarrow \gamma\chi_{c2})$	$9.621 \pm 0.013 \pm 0.272$	$9.33 \pm 0.14 \pm 0.61$ [9]	8.8 ± 0.5	9.11 ± 0.31
$\mathcal{B}(\psi(3686) \rightarrow \gamma\chi_{c0}) \times \mathcal{B}(\chi_{c0} \rightarrow \gamma J/\psi)$	$0.024 \pm 0.015 \pm 0.205$	$0.125 \pm 0.007 \pm 0.013$ [31] $0.151 \pm 0.003 \pm 0.010$ [15] $0.158 \pm 0.003 \pm 0.006$ [16]	0.131 ± 0.035	0.127 ± 0.006
$\mathcal{B}(\psi(3686) \rightarrow \gamma\chi_{c1}) \times \mathcal{B}(\chi_{c1} \rightarrow \gamma J/\psi)$	$3.442 \pm 0.010 \pm 0.132$	$3.56 \pm 0.03 \pm 0.12$ [31] $3.377 \pm 0.009 \pm 0.183$ [15] $3.518 \pm 0.01 \pm 0.120$ [16]	2.93 ± 0.15	3.24 ± 0.07
$\mathcal{B}(\psi(3686) \rightarrow \gamma\chi_{c2}) \times \mathcal{B}(\chi_{c2} \rightarrow \gamma J/\psi)$	$1.793 \pm 0.008 \pm 0.163$	$1.95 \pm 0.02 \pm 0.07$ [31] $1.874 \pm 0.007 \pm 0.102$ [15] $1.996 \pm 0.008 \pm 0.070$ [16]	1.52 ± 0.15	1.75 ± 0.04
$\mathcal{B}(\chi_{c0} \rightarrow \gamma J/\psi)$	$0.25 \pm 0.16 \pm 2.15$	$2 \pm 0.2 \pm 0.2$ [32]		1.27 ± 0.06
$\mathcal{B}(\chi_{c1} \rightarrow \gamma J/\psi)$	$34.75 \pm 0.11 \pm 1.70$	$37.9 \pm 0.8 \pm 2.1$ [32]		33.9 ± 1.2
$\mathcal{B}(\chi_{c2} \rightarrow \gamma J/\psi)$	$18.64 \pm 0.08 \pm 1.69$	$19.9 \pm 0.5 \pm 1.2$ [32]		19.2 ± 0.7

TABLE V. Partial widths (keV) of radiative transitions for $\psi(3686) \rightarrow \gamma J/\psi$ and $\chi_{cJ} \rightarrow \gamma J/\psi$. Shown are our experimental results and predictions from a relativistic quark model (RQM) [33]; non-relativistic potential and Godfrey-Isgur relativized potential models (NR/GI) [34]; color screened models [35], calculated with zeroth order wave functions (SNR₀) and first order relativistically corrected wave functions (SNR₁); and linear potential (LP) and screened potential models (SP) [8]. The Γ_{E1} predictions include only $E1$ transition calculations, while the Γ_{EM} results include higher order multipole corrections.

Initial state	Final state	Γ_{E1} (keV)					Γ_{EM} (keV)		
		RQM [33]	NR/GI [34]	SNR _{0/1} [35]	LP [8]	SP [8]	LP [8]	SP [8]	This analysis
$\psi(3686)$	χ_{c0}	26.3	63/26	74/25	27	26	22	22	26.9 ± 1.8
	χ_{c1}	22.9	54/29	62/36	45	48	42	45	28.3 ± 1.9
	χ_{c2}	18.2	38/24	43/34	36	44	38	46	27.5 ± 1.7
χ_{c0}	J/ψ	121	152/114	167/117	141	146	172	179	
		265	314/239	354/244	269	278	306	319	306 ± 23
		327	424/313	473/309	327	338	284	292	363 ± 41

are listed in Table IV. Our $\psi(3686) \rightarrow \gamma\chi_{cJ}$ branching fractions are the most precise. The branching fractions for $\psi(3686) \rightarrow \gamma\chi_{cJ}$ agree with CLEO within one standard deviation, except for $\psi(3686) \rightarrow \gamma\chi_{c1}$ which differs by 1.3 standard deviations. The product branching fractions $\mathcal{B}(\psi(3686) \rightarrow \gamma\chi_{c1}) \times \mathcal{B}(\chi_{c1} \rightarrow \gamma J/\psi)$ and $\mathcal{B}(\psi(3686) \rightarrow \gamma\chi_{c2}) \times \mathcal{B}(\chi_{c2} \rightarrow \gamma J/\psi)$ agree with the previous BESIII measurements. Because of the difficulty in fitting $\psi(3686) \rightarrow \gamma\chi_{c0}, \chi_{c0} \rightarrow \gamma J/\psi$, our product branching fraction has a very large systematic error compared with those using exclusive decays.

Partial widths are shown in Table V. For comparison with models, experimental results have become accurate enough (partly due to this measurement) to become sensitive to fine details of the potentials, e.g. relativistic effects, screening effects, and higher partial waves.

XI. ACKNOWLEDGMENTS

The BESIII collaboration thanks the staff of BEPCII and the IHEP computing center for their strong support. This work is supported in part by National Key Basic Research Program of China under Contract No. 2015CB856700; National Natural Science Foundation of China (NSFC) under Contracts Nos. 11235011, 11322544, 11335008, 11425524, 11635010; the Chinese Academy of Sciences (CAS) Large-Scale Scientific Facility Program; the CAS Center for Excellence in Particle Physics (CCEPP); the Collaborative Innovation Center for Particles and Interactions (CICPI); Joint Large-Scale Scientific Facility Funds of the NSFC and CAS under Contracts Nos. U1232201, U1332201; CAS under Contracts Nos. KJCX2-YW-N29, KJCX2-YW-N45; 100 Talents Program of CAS; National 1000 Talents Program of China; INPAC and Shanghai Key Laboratory for Particle Physics and Cosmology; German Research Foun-

dation DFG under Contracts Nos. Collaborative Research Center CRC 1044, FOR 2359; Istituto Nazionale di Fisica Nucleare, Italy; Joint Large-Scale Scientific Facility Funds of the NSFC and CAS under Contract No. U1532257; Joint Large-Scale Scientific Facility Funds of the NSFC and CAS under Contract No. U1532258; Koninklijke Nederlandse Akademie van Wetenschappen (KNAW) under Contract No. 530-4CDP03; Ministry of Development of Turkey under Contract No. DPT2006K-120470; National Natural Science Foundation of China (NSFC) under Contract No. 11575133; National Science and Technology fund; NSFC under Contract No. 11275266; The Swedish Research Council; U. S. Department of Energy under Contracts Nos. DE-FG02-05ER41374, DE-SC-0010504, DE-SC0012069; University of Groningen (RuG) and the Helmholtzzentrum fuer Schwerionenforschung GmbH (GSI), Darmstadt; WCU Program of National Research Foundation of Korea under Contract No. R32-2008-000-10155-0

-
- [1] M. Riordin, *The Hunting of the Quark*, New York, Simon and Schuster (1987).
- [2] N. Brambilla *et al.* (Quarkonium Working Group Collaboration), CERN-2005-005, CERN Geneva (2005), arXiv:hep-ph/0412158.
- [3] W. Braunschweig *et al.* (DASP Collaboration), Phys. Lett. B **57**, 407 (1975).
- [4] G. J. Feldman *et al.*, Phys. Rev. Lett. **35**, 821 (1975), [Erratum-ibid. **35**, 1184 (1975)].
- [5] E. Eichten *et al.*, Phys. Rev. Lett. **34**, 369 (1975) [Erratum-ibid. **36**, 1276 (1976)].
- [6] T. Appelquist *et al.*, Phys. Rev. Lett. **34**, 365 (1975).
- [7] C. Patrignani *et al.* (Particle Data Group), Chin. Phys. C **40**, 100001 (2016).
- [8] W. J. Deng, H. Liu, L. C. Gui, and X. H. Zhong, Phys. Rev. D, **95**, 034026 (2016).
- [9] S. B. Athar *et al.* (CLEO Collaboration), Phys. Rev. D **70**, 112002 (2004).
- [10] J. E. Gaiser *et al.* (Crystal Ball Collaboration), Phys. Rev. D **34**, 711 (1986).
- [11] M. Ablikim *et al.* (BESIII Collaboration), Phys. Rev. D **88**, 032007 (2013).
- [12] M. Ablikim *et al.* (BESIII Collaboration), Phys. Rev. D **86**, 092008 (2012).
- [13] M. Ablikim *et al.* (BESIII Collaboration), Phys. Rev. Lett. **104**, 132002 (2010).
- [14] M. Ablikim *et al.* (BESIII Collaboration), Phys. Rev. D **86**, 092009 (2012).
- [15] M. Ablikim *et al.* (BESIII Collaboration), Phys. Rev. Lett. **109**, 172002 (2012).
- [16] M. Ablikim *et al.* (BESIII Collaboration), Phys. Rev. D **95**, 072004 (2017).
- [17] M. Ablikim *et al.* (BESIII Collaboration), Chin. Phys. C **37**, 063001 (2013).
- [18] D. M. Asner *et al.*, Int. J. Mod. Phys. A **24**, 499 (2009).
- [19] M. Ablikim *et al.* (BESIII Collaboration), Nucl. Instrum. Meth. A **614**, 345 (2010).
- [20] S. Agostinelli *et al.* (GEANT4 Collaboration), Nucl. Instrum. Meth. A **506**, 250 (2003).
- [21] Z. Y. Deng *et al.*, Chin. Phys. C **30**, 371 (2006).
- [22] S. Jadach, B. F. L. Ward, and Z. Was, Comput. Phys. Commun. **130**, 260 (2000).
- [23] S. Jadach, B. F. L. Ward, and Z. Was, Phys. Rev. D **63**, 113009 (2001).
- [24] E. Barberio and Z. Was, Comput. Phys. Commun. **79**, 291 (1994).
- [25] D. J. Lange, Nucl. Instrum. Meth. A **462**, 152 (2001); R. G. Ping *et al.*, Chin. Phys. C **32**, 599 (2008).
- [26] J. C. Chen, G. S. Huang, X. R. Qi, D. H. Zhang, and Y. S. Zhu, Phys. Rev. D **62**, 034003 (2000).
- [27] G. Karl, S. Meshkov, and J. L. Rosner, Phys. Rev. D **13**, 1203 (1976); M. A. Doncheski, H. Grotch, and K. J. Sebastian, *ibid* **42** 2293 (1990).
- [28] G. R. Liao, R. G. Ping, and Y. X. Yong, Chin. Phys. C **26**, 051101 (2009).
- [29] E. Eichten, S. Godfrey, H. Mahlke, and J. L. Rosner, Rev. Mod. Phys. **80**, 1161, (2008).
- [30] M. Ablikim *et al.* (BESIII Collaboration), Phys. Rev. D **83**, 112005 (2011).
- [31] H. Mendez *et al.* (CLEO Collaboration), Phys. Rev. D **78**, 011102 (2008).
- [32] N. E. Adam *et al.* (CLEO Collaboration), Phys. Rev. Lett. **94**, 232002 (2005).
- [33] D. Ebert, R. N. Faustov, and V. O. Galkin, Phys. Rev. D **67**, 014027 (2003).
- [34] T. Barnes, S. Godfrey, and E. S. Swanson, Phys Rev D **72**, 054026 (2005).
- [35] B. Q. Li and K. T. Chao, Phys. Rev. D **79**, 094004 (2009).